

Article

Structural Evolution of Molybdenum Carbides in Hot Aqueous Environments and Impact on Low-Temperature Hydroprocessing of Acetic Acid

Jae-Soon Choi ^{1,*}, Viviane Schwartz ¹, Eduardo Santillan-Jimenez ², Mark Crocker ², Samuel A. Lewis Sr. ¹, Michael J. Lance ¹, Harry M. Meyer III ¹ and Karren L. More ¹

¹ Oak Ridge National Laboratory, 1 Bethel Valley Road, Oak Ridge, TN 37831, USA; E-Mails: schwartzv@ornl.gov (V.S.); lewissasr@ornl.gov (S.A.L.); lancem@ornl.gov (M.J.L.); meyerhmiii@ornl.gov (H.M.M.); morekl1@ornl.gov (K.L.M.)

² University of Kentucky Center for Applied Energy Research, 2540 Research Park Drive, Lexington KY 40511, USA; E-Mails: e.santillan@uky.edu (E.S.-J.); mark.crocker@uky.edu (M.C.)

* Author to whom correspondence should be addressed; E-Mail: choijs@ornl.gov; Tel.: +1-865-946-1368; Fax: +1-865-946-1354.

Academic Editor: Keith Hohn

Received: 8 January 2015 / Accepted: 6 March 2015 / Published: 13 March 2015

Abstract: We investigated the structural evolution of molybdenum carbides subjected to hot aqueous environments and their catalytic performance in low-temperature hydroprocessing of acetic acid. While bulk structures of Mo carbides were maintained after aging in hot liquid water, a portion of carbidic Mo sites were converted to oxidic sites. Water aging also induced changes to the non-carbidic carbon deposited during carbide synthesis and increased surface roughness, which in turn affected carbide pore volume and surface area. The extent of these structural changes was sensitive to the initial carbide structure and was lower under actual hydroprocessing conditions indicating the possibility of further improving the hydrothermal stability of Mo carbides by optimizing catalyst structure and operating conditions. Mo carbides were active in acetic acid conversion in the presence of liquid water, their activity being comparable to that of Ru/C. The results suggest that effective and inexpensive bio-oil hydroprocessing catalysts could be designed based on Mo carbides, although a more detailed understanding of the structure-performance relationships is needed, especially in upgrading of more complex reaction mixtures or real bio-oils.

Keywords: molybdenum carbide; Mo₂C; biomass; bio-oil; pyrolysis oil; hydroprocessing; acetic acid hydrogenation; heterogeneous catalysis

1. Introduction

Fast pyrolysis is an efficient and inexpensive method to produce liquids from lignocellulosic biomass. However, the liquid products (so-called bio-oils) are not suitable for direct application as fuels in internal combustion engines due to their high content of oxygen (35–40 wt.%, dry basis) and water (15–30 wt.%) [1]. For instance, various oxygenated hydrocarbon species present in raw bio-oils make these liquids unstable for long-term storage, corrosive, low in heating value, and poorly miscible with conventional hydrocarbon fuels. In particular, bio-oils can contain a large amount of formic and acetic acids which must be converted to less corrosive species to improve the overall compatibility of the liquid with the current petroleum-based transportation fuel infrastructure [2].

The quality of bio-oils can be improved by eliminating oxygenated functionalities, hydroprocessing being one of the most promising upgrading strategies. Hydroprocessing is a well-established and widely employed operation in current petroleum refineries [3]. A major advantage of applying hydroprocessing to bio-oils is the relatively high yield of liquid fuels and a high degree of carbon atom retention [4,5]. Much of the research done thus far has involved well-established petroleum refinery catalysts, such as alumina-supported CoMo or NiMo sulfides [6]. However, extrapolating the use of sulfides to bio-oils has proven challenging due to the instability of sulfides under bio-oil upgrading conditions. Indeed, given the low sulfur content of bio-oils, the addition of sulfiding agents to the bio-oil feed is necessary to maintain active sulfide phases, a practice that risks contaminating the products with sulfur. Hydrothermal aging – which can cause phase changes in catalyst supports [7]—is another potential deactivation route as water represents a major byproduct of hydrodeoxygenation and raw bio-oils contain a significant amount of water (~25%).

Due to highly reactive oxygenated species present in raw bio-oils—such as olefins, aldehydes and ketones—extensive polymerization occurs at typical hydroprocessing temperatures (370–400 °C) leading to rapid coking and fouling of catalyst beds [8]. To circumvent this problem, the current state of the art (at various R&D stages) generally employs multiple sequential hydroprocessing steps. A common practice is to stabilize bio-oils at low temperatures (150–200 °C) over an efficient hydrogenation catalyst (e.g., Ru/C) followed by high temperature (370–400 °C) deep deoxygenation and hydrocracking over sulfided CoMo or NiMo catalysts [9,10]. Despite the relatively good activity of Ru/C in the low-temperature hydrogenation (stabilization) of bio-oils, Ru catalysts tend to generate fully hydrogenated compounds, as well as gasification products consuming excessive amounts of H₂ [11]. High cost of Ru metal utilization is another issue. Hence, despite the progress made to date, it is desirable to design novel catalysts tailored specifically to bio-oils, with an emphasis on avoiding the use of precious metals and improving durability *vis-à-vis* state-of-the-art catalysts.

Transition-metal carbides (TMCs) have been investigated extensively as potential substitutes for precious metal catalysts, since early studies found that TMCs manifest catalytic behaviors typically observed with Pt-group metal catalysts in several hydrocarbon conversion reactions [12–14]. For

example, Mo₂C is often compared with Ru in hydrogenation reactions [14–16]. As Mo carbides can be prepared with high-surface area [17,18], they can be deployed as “bulk” catalysts without using support materials. This simple catalyst design could in turn be advantageous when one tries to further enhance the structural stability of catalysts. By contrast, for supported catalysts such as Ru/C, the stability of the various components (active phases, supports and interfaces) needs to be considered.

Based on these considerations, Mo₂C appears to be a good candidate as a low-cost alternative to Ru/C catalysts for the low-temperature hydroprocessing of bio-oils. While there are recent studies focused on evaluating Mo carbides as catalysts for biomass upgrading [19–22], little has been done to investigate Mo₂C in the context of bio-oil low-temperature hydroprocessing, particularly in terms of their hydrothermal stability. In this work, the main focus was placed on evaluating the hydrothermal stability of the carbide catalysts. To this end, we prepared and compared two Mo₂C samples exposed to hot aqueous environments, probing if and how differences in initial structure affected their hydrothermal stability and intrinsic catalyst activity in the aqueous-phase hydroprocessing of acetic acid. Initial results are promising, suggesting that it is possible to design robust and active catalysts for low-temperature bio-oil hydroprocessing using inexpensive Mo carbides.

2. Results and Discussion

2.1. Synthesis and Characterization of Mo Carbides

Ammonium heptamolybdate is a precursor widely used for Mo carbide synthesis [22,23]. Effluent gas analysis performed with a mass spectrometer (Figure S1A) afforded gas concentration profiles typical of carburization processes involving this type of Mo precursor: reduction to MoO₂ mainly by H₂, followed by simultaneous O removal and C insertion at higher temperatures [16,18,23]. As expected, the carburization product, which we denote here as Mo₂C-A, presented a hexagonal close packed (hcp) Mo₂C structure (Figure 1).

The Mo₂C-B was prepared under the same conditions as the Mo₂C-A, but using an oxide precursor synthesized with a block copolymer templating method. The reason for using this unconventional precursor was to obtain a Mo₂C with a structure distinct from that of Mo₂C-A and thus help understand if structural differences could affect the catalyst performance in hot aqueous environments. This precursor was unconventional in that even though the ratio of O/Mo (2.8) was close to the theoretical value for MoO₃ (see XPS results in Table S1), the precursor contained a large amount of carbon and exhibited a crystallographically amorphous structure (Figure S2). The reduction-carburization behavior of this precursor was unique as well, with considerable C involvement (likely from the precursor) during the low temperature reduction period (see CO, CO₂ formation in Figure S1B). The resulting crystallographic structure of Mo₂C-B differed somewhat from that of Mo₂C-A even though the overall structure was hcp for both samples (Figure 1). Indeed, when crystallite sizes were estimated from peak broadening (using the Scherrer equation), the values for the two major planes (101) and (110) of Mo₂C-A were close to one another (11 nm, Table 1), while for Mo₂C-B, values of 13 and 19 nm were obtained, respectively, for (101) and (110) planes. It appears, therefore, that the crystallite shape of Mo₂C-B differed from what is commonly observed for “conventional” Mo₂C such as Mo₂C-A [18].

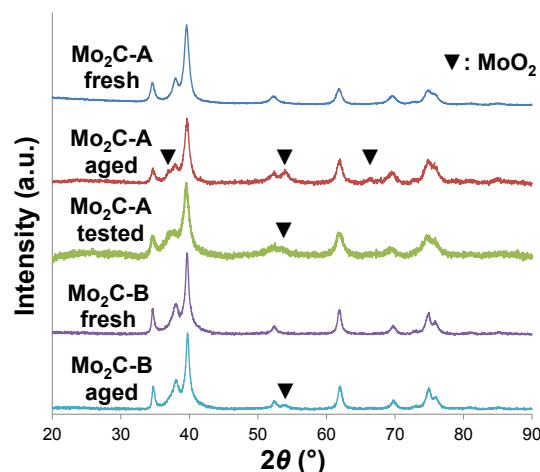


Figure 1. XRD patterns of two Mo₂C samples (A and B) before and after aging for 48 h in hot liquid water. The pattern for Mo₂C-A obtained after a 48 h aqueous-phase hydroprocessing run (10% guaiacol in water as feed) is also presented for comparison (Mo₂C-A tested).

Previous studies have shown that the primary particles of Mo₂C prepared under carburization conditions similar to those employed in the present work, are single crystals [16,18]. Consequently, crystallite sizes determined using XRD data are close to the particle sizes estimated from BET surface area as long as access to the primary particle surface is not blocked by bulk carbon deposited during the carburization. As both Mo₂C-A and Mo₂C-B in fresh state presented larger particle sizes than the calculated crystallite sizes in the present work (Table 1), it can be concluded that there was significant bulk carbon deposition during the carbide synthesis which prevented the passage of the N₂ probe molecules through the micropores during BET measurements. The presence of non-carbidic C was confirmed by XPS analysis (see C_{cont} in Table 2 and Figure S3), but the impact of the bulk carbon deposition was especially important for Mo₂C-B, which presented significantly smaller BET surface (*i.e.*, larger estimated particle sizes) and pore volume than Mo₂C-A, in spite of the comparable crystallite sizes.

Structural differences between the two Mo₂C samples can be found at the grain level as well. The SEM images in Figure 2 reveal that each carbide inherited a distinct grain morphology from its oxide precursor. For example, Mo₂C-B grains had sharper edges and corners and were significantly flatter than those of Mo₂C-A. Higher magnification imaging showed similar morphological differences for smaller particles (Figure 3), which seems to be consistent with the anisotropic XRD peak broadening discussed above.

Another catalytically relevant carbide property worth discussing is the density of active sites determined from CO uptake and BET surface area measurements (Table 1). The site density determined in this way is generally higher when residual oxygen is minimized and carbidic carbon insertion is more complete while bulk carbon deposition is prevented [16,18]. The fact that Mo₂C-B had an inferior site density despite the higher extent of carburization (inferred from C/Mo of carbide phases in Table 2) indicates that a larger portion of active sites were likely blocked by non-carbidic C. Despite the relatively comparable C_{cont} content (Table 2), greater blockage of both pores and active sites apparently occurred over Mo₂C-B than Mo₂C-A. One possible explanation is differences in type and shape of the non-carbidic C species deposited on the two carbides.

Table 1. BET surface area, pore volume, pore size, CO uptake, density of sites, particle size and crystallite size of the catalysts studied.

Catalyst	BET surface area, $S_g/m^2 g^{-1}$	Pore volume $/cm^3 g^{-1}$	Pore size $/nm$	CO uptake $/\mu mol g^{-1}$	Site density ^a $/\times 10^{15} cm^{-2}$	Particle size, D_p ^b $/nm$	Crystallite size, D_c ^c $/nm$
Mo ₂ C-A fresh	36	0.08	8	186	0.31	18	11/11
Mo ₂ C-A aged	64	0.50	36	26	0.02	10	10/11
Mo ₂ C-A tested	22	0.02	4	186	0.51	30	8/10
Mo ₂ C-B fresh	6	0.03	23	5	0.05	110	13/19
Mo ₂ C-B aged	15	0.02	4	12	0.05	44	12/16
Ru/C fresh	815	NM ^d	NM ^d	NA ^e	0.04 ^f	1.1 ^g	NA ^e
Ru/C aged	765	NM ^d	NM ^d	NA ^e	0.01 ^f	2.0 ^g	NA ^e

^a CO uptake normalized to BET surface area; ^b Estimated from BET surface area; ^c Estimated from XRD peak broadening: (101) plane/(110) plane; ^d Not measured; ^e Not applicable; ^f Number of exposed Ru atoms (estimated from particle sizes) normalized to BET surface area; ^g Measured by TEM.

Table 2. Surface composition of Mo₂C catalysts analyzed by XPS ^a.

Catalyst	Mo _{carb} ^b $/at. \%$	Mo _{oxid} ^c $/at. \%$	C _{carb} ^b $/at. \%$	C _{cont} ^d $/at. \%$	O _{oxid} ^c $/at. \%$	O _{cont} ^d $/at. \%$	C/Mo ^e	O/Mo ^f
Mo ₂ C-A fresh	31.5	6.4	9.9	16.2	25.7	10.5	0.31	4.03
Mo ₂ C-A aged	8.3	24.1	1.4	4.4	34.8	27.0	0.17	1.44
Mo ₂ C-A tested	13.2	14.6	4.4	31.8	22.3	13.8	0.33	1.53
Mo ₂ C-B fresh	40.0	4.8	15.7	13.5	14.5	11.5	0.39	3.02
Mo ₂ C-B aged	17.7	9.5	4.8	15.3	28.8	23.9	0.27	3.03

^a Measurements done after Ar sputtering; ^b Carbides; ^c Oxides; ^d Contaminants, meaning that elements are not associated with carbide or oxide phases; ^e C/Mo ratio of surface carbide phases (theoretical value for bulk Mo₂C is 0.5); ^f O/Mo ratio of surface oxide phases.

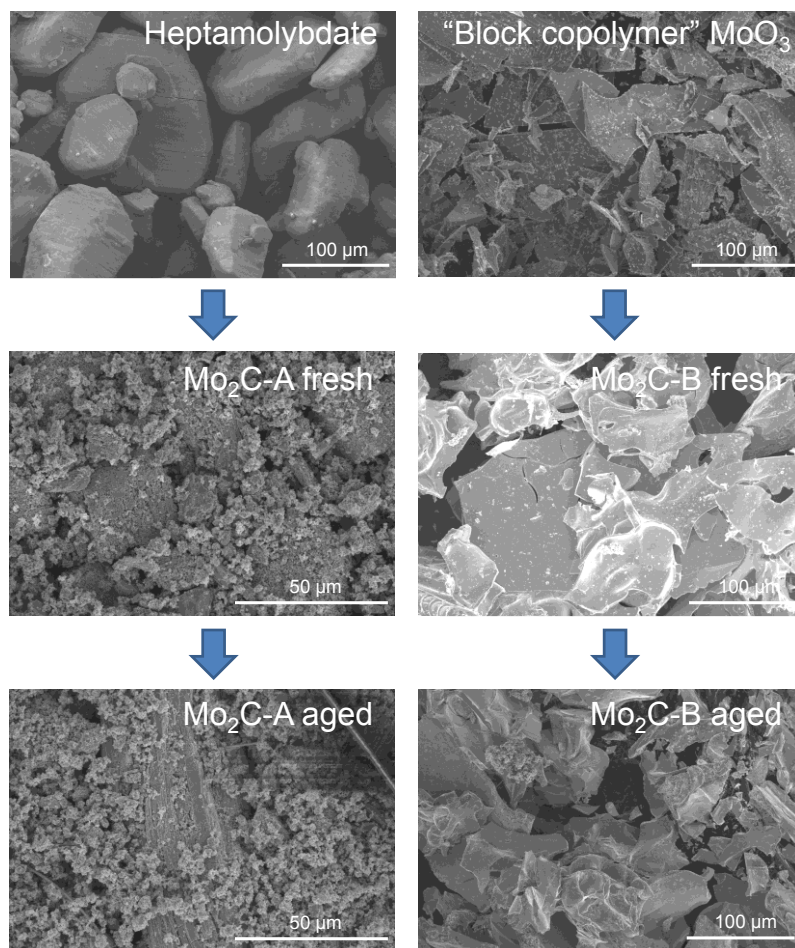


Figure 2. SEM images of the two Mo oxide precursors and resulting carbide samples before and after 48 h aging at 250 °C in liquid water.

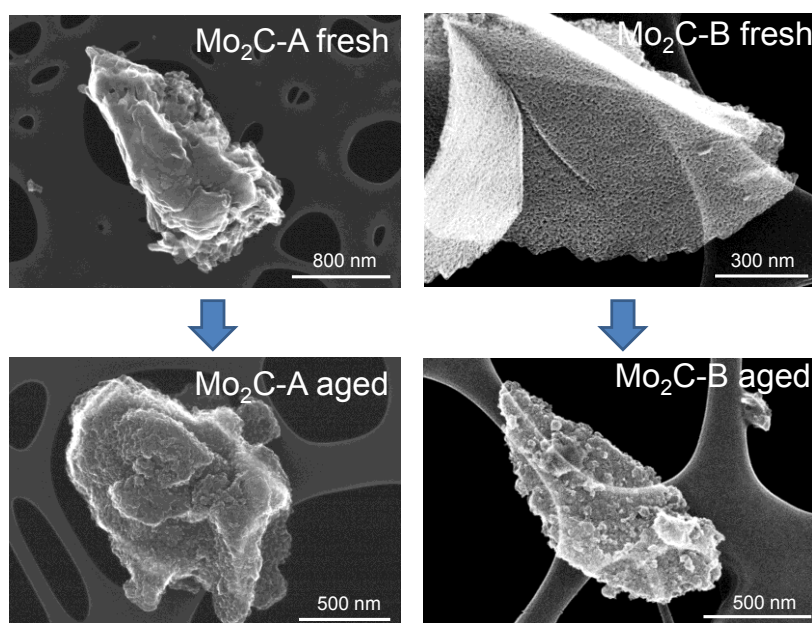


Figure 3. SEM images of two Mo₂C samples in the fresh state and after 48 h aging at 250 °C in liquid water; smaller particles taken at high magnification.

2.2. Structural Evaluation of Mo Carbides Subjected to Hot Aqueous Environments

An important technical challenge facing the development of catalysts for biomass conversion processes is the hydrothermal instability of conventional catalytic materials. For instance, γ -Al₂O₃, a popular support used in petroleum refineries for metal sulfide and precious metal catalysts, is rapidly hydrated and converted to boehmite in hot liquid water [7,24]. For the two Mo carbide samples studied in this work, despite the extended exposure to hydrothermally challenging environments (liquid water, 250 °C, 48 h), the overall bulk structure was maintained (e.g., hcp crystallographic structure and grain morphology as shown in Figures 1 and 2, respectively). This is an encouraging observation in view of the aforementioned necessity of novel catalytic materials for biomass conversion processes. Detailed characterization, however, revealed that some significant structural changes occurred on both Mo₂C-A and Mo₂C-B samples. For instance, a portion of the carbide phases were converted into MoO₂ phases as detected by XRD (Figure 1). The high oxygen affinity of Mo carbides is well documented in the literature [25], and our present results show that liquid-phase H₂O can also oxidize Mo carbides.

The fact that a considerable fraction of the carbidic (MoC_x) sites on the surface of both samples were converted into oxidic (MoO_x) sites was confirmed by XPS (Table 2). Interestingly, the number of carbidic sites (in terms of at.%) not only decreased, but the remaining carbidic sites also lost some of their C neighbors and instead gained O—as suggested by the fact that the C/Mo ratio of the carbide phases within Mo₂C-A, for instance, decreased from 0.31 to 0.17 while the content of O contaminant (*i.e.*, O not related to Mo oxides) increased from 25.7 to 34.8 at.%.

As mentioned above, it is well known that the composition of Mo sites plays a critical role in determining the surface reactivity of Mo carbides as measured by CO chemisorption [16,26]. It is thus unsurprising that the surface oxidation of Mo₂C-A led to decreased CO uptake and site density (Table 2). Given that Mo₂C-B also suffered surface oxidation, one would expect to see a similar trend. Instead, CO uptake on Mo₂C-B actually increased. This discrepancy might be related to the fact that only a fraction of “active” sites were exposed (*i.e.*, able to adsorb CO) over the fresh Mo₂C-B due to non-carbidic C deposition as discussed above. As the surface morphology changed considerably due to hydrothermal aging, it seems reasonable to conjecture that the number of exposed active sites slightly increased. Despite the increase, one should note that the CO uptake by Mo₂C-B was still much lower than those typically observed for Mo carbides prepared under similar conditions, including Mo₂C-A. Moreover, the extent of surface oxidation was relatively small for the Mo₂C-B sample. Another intriguing difference is that the surface C_{cont.} increased for Mo₂C-B, meaning that a portion of the C removed from MoC_x sites (C_{carb.}) was retained on the surface as non-carbidic C species (C_{cont.}). The retention of C might have helped maintain surface hydrophobicity, which would in turn have mitigated oxidation by H₂O.

The BET surface area increased after water aging for both samples (Table 1). In the case of Mo₂C-A, the concomitant increase in pore size and volume and decrease in C_{cont.} (Table 2) indicates that bulk (non-carbidic) C deposits blocking carbide pores were removed during hot water aging. This interpretation is supported by the fact that—after aging—the particle size estimated from BET surface area matched the crystallite size obtained from XRD data (Table 1). Again, Mo₂C-B appears to have responded differently to hydrothermal aging, as the increased surface area was not accompanied by an increase in porosity. Instead, the pore volume of this sample decreased, which is consistent with the

gain in C_{cont} (Table 2), meaning that more bulk C (C_{cont}) was involved in pore blocking. The FIB-SEM images in Figure 4 seem to agree with this interpretation. The intra-grain images confirm that the aging increased pore openings for Mo₂C-A, while it decreased those for Mo₂C-B (in terms of both number and size).

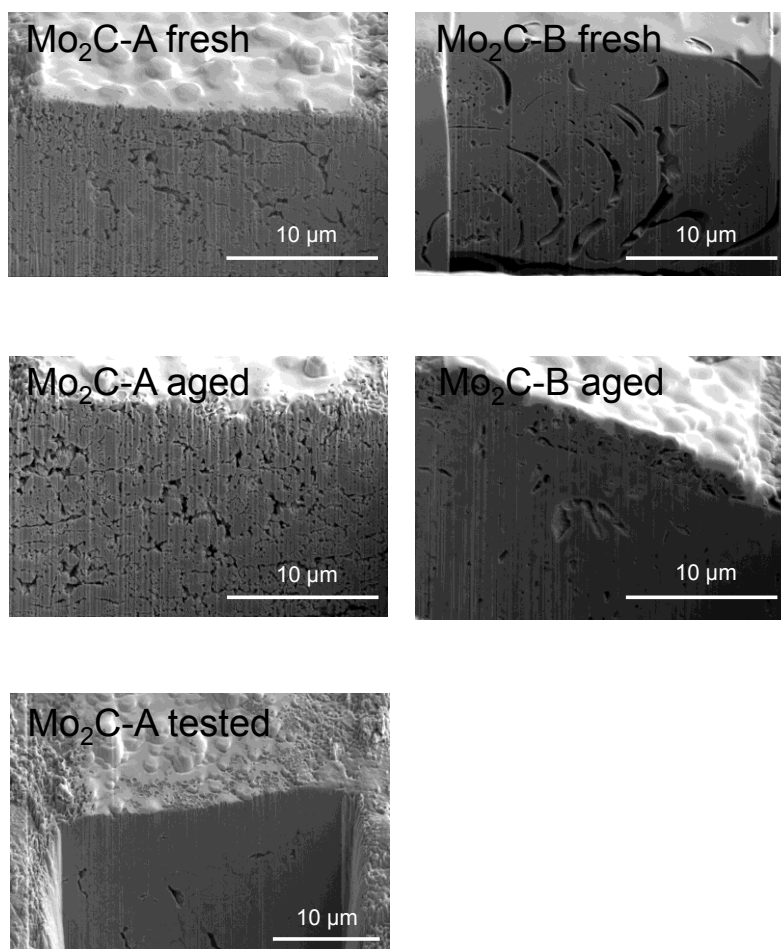


Figure 4. FIB-SEM images of the two Mo₂C samples (A and B) before and after aging for 48 h in hot liquid water. The image for Mo₂C-A obtained after a 48 h aqueous-phase hydroprocessing run (10% guaiacol in water as feed) is also presented for comparison (Mo₂C-A tested).

When Mo₂C-A was tested for 48 h at the same temperature (250 °C) but under actual hydroprocessing conditions (10% guaiacol in water + H₂), both pore opening and BET surface area decreased, likely due to increased C_{cont} as in the case of Mo₂C-B (see Figure 4 and Tables 1 and 2). Despite the BET surface area loss due to pore blocking, Mo₂C-A maintained the same degree of CO uptake after testing (Table 1). As mentioned above, the number of metallic sites measured for Mo₂C-B also did not degrade with aging and actually increased. The C from guaiacol molecules and non-carbidic C thus appear to have had similar effects with respect to mitigating H₂O-induced bulk oxidation of Mo₂C-A and Mo₂C-B, respectively (see lower bulk MoO₂ detected by XRD in Figure 1). Similar beneficial effects, *i.e.*, preventing hydration and metal particle agglomeration, have been

reported for carbonaceous surface species derived from biomass compounds dissolved in liquid water over alumina catalysts [27].

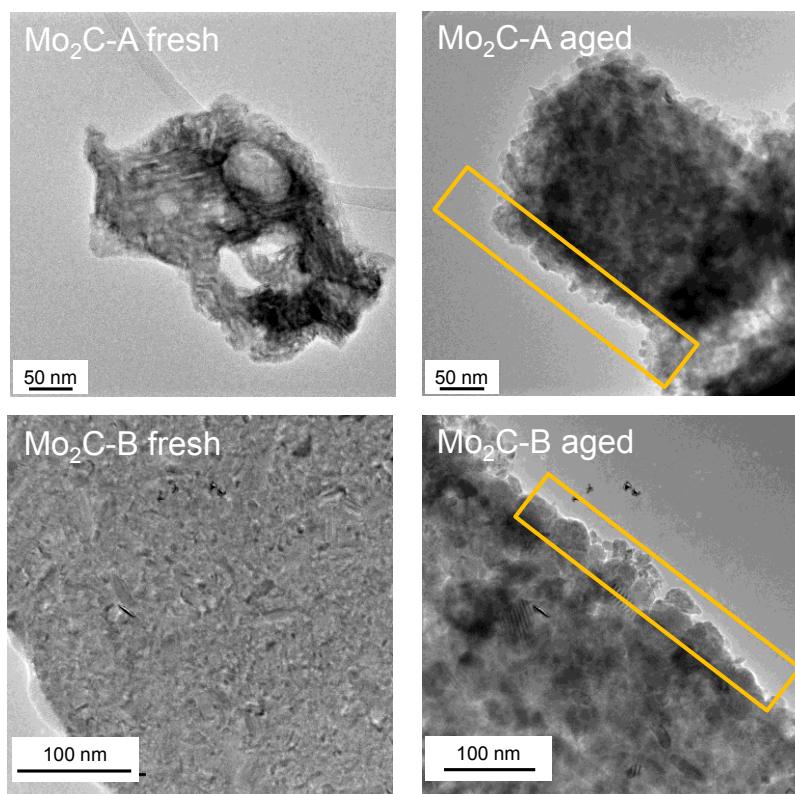


Figure 5. TEM images of Mo carbides in the fresh state and after 48 h aging at 250 °C in liquid water; the yellow boxes highlight increased surface roughness due to the formation of elliptically shaped particles.

The surface area increase of Mo₂C-B despite the pore blocking could be explained by increased surface roughness. Liquid water aging developed nanoparticles of elliptical shape on the surface of both carbide samples (Figures 5 and S4). These small particles were mainly Mo oxides in agreement with the XPS data (Table 2). Since Mo₂C-B sample initially had a lower surface area than Mo₂C-A sample (36 vs. 6 m²/g) and experienced pore blocking during aging, the impact of the increased roughness on BET surface area might be discernible. In contrast, the pore opening due to water aging led to a dramatic increase in surface area for Mo₂C-A (36 to 64 m²/g), masking the relatively small contribution of the roughness-induced surface area increase.

In summary, Mo carbides maintained overall bulk structures under hydrothermally harsh environments, but can undergo H₂O-induced oxidation. An important lesson that can be learned from these results is that the extent of oxidation can be minimized by controlling Mo carbide structure. The superior oxidation resistance of the Mo₂C-B structure compared to Mo₂C-A is further confirmed by TGA performed in air (Figure 6), in which Mo₂C-B exhibited oxidation onset temperatures (*i.e.*, temperatures at which significant weight gain started) at least 100 °C higher than Mo₂C-A.

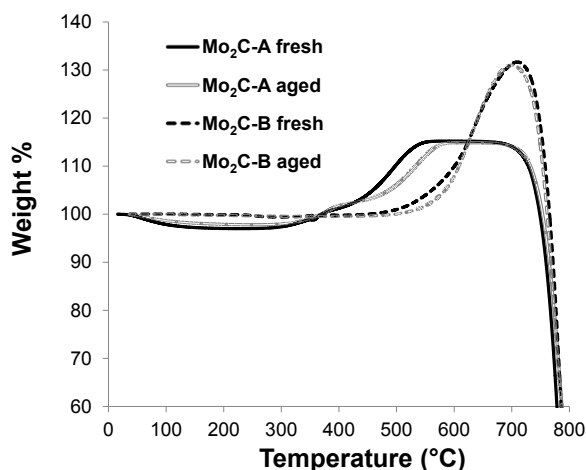


Figure 6. TGA profiles of two Mo₂C samples in the fresh state and after 48 h aging at 250 °C in liquid water. Temperature increased from room temperature to 800 °C at 10 °C/min in air (25 mL/min). The solid and dashed lines correspond to the relative weight change of Mo₂C-A and Mo₂C-B samples, respectively.

2.3. Catalytic Performance in Aqueous-Phase Hydroprocessing of Acetic Acid

To assess the catalytic effectiveness of Mo carbides in converting oxygenates in liquid water, Mo₂C-A and Mo₂C-B were evaluated using a 10 wt.% solution of acetic acid in water. This model reaction was chosen considering the fact that pyrolysis oils can contain a large amount of organic acids including acetic acid [2], and this type of model compound testing has been used previously to study the hydroprocessing performance of Ru/C and Pd/C (catalysts commonly used to stabilize bio-oils via low temperature hydroprocessing) [11]. A commercial 5% Ru/C was also evaluated before and after a 48 h water aging for comparison purposes. Carbon supports are widely studied in the context of water-based catalytic processes due to their relative hydrothermal stability [28] and Ru is one of the best catalysts known for acetic acid hydrogenation [29,30] and low-temperature processing (stabilization) of bio-oil [6,9]. Some catalytically relevant properties of the 5% Ru/C reference catalyst are reported in Tables 1 and S2, and Figure S5. Briefly, the surface area of Ru/C decreased slightly during hydrothermal aging, while the average particle size doubled. Based on XPS, the surface Ru content decreased from 4.2 to 1.9 at.% likely due to metal leaching. This result further highlights the challenging nature of catalyst development for biomass conversion. Conversion values as well as average rates obtained in the present study are compiled in Table 3. Note that the product analysis was done only at the end of each 4 h run, therefore the conversion rate represents the apparent average activity of a catalyst. It is possible that some other deactivation mechanisms (e.g., coking during 4 h hydroprocessing) contributed to the average conversion rates. Further research using steady state flow reactor experiments could help obtain more accurate activity data and comparison among different catalysts. Another parameter which could have influenced the activity measurements is the possible effect of internal mass transfer, as the catalysts studied in this work presented significantly different particle sizes (Table 1). Olcay *et al.* calculated the Weisz Modulus for an aqueous-phase hydrogenation of acetic acid over a Ru/C catalyst; the obtained 10^{-15} was well below the limit value of 0.15 (that is, the kinetic measurements were done in the absence of mass transport limitation) [29].

Considering that our reaction conditions were quite similar to those used in [29], we could estimate that our Ru/C catalyst was evaluated also without mass transport limitation. More detailed and rigorous kinetic experiments and catalyst morphology characterization are needed to address this question for Mo carbides.

All of the catalysts were active in acetic acid conversion at 200 and 250 °C (Table 3). The Ru/C catalyst converted more molecules of acetic acid per catalyst mass than Mo₂C. However, if the comparison is done on the intrinsic activity basis (*i.e.*, number of converted acetic acid molecules per surface area), the activity of Mo₂C-B was comparable to that of Ru/C. Considering that the Mo₂C-B sample had a relatively low BET surface area for a carbide prepared via a temperature programmed method, one could envision that the performance (mass basis) of Mo₂C could be significantly improved by increasing total surface area while maintaining the properties of the catalytic surface. In comparison, the metal dispersion of the Ru/C (over 80%) was already quite close to the theoretical maximum. Between the two Mo carbides, the intrinsic activity of fresh Mo₂C-B was 3–4 times higher than that of fresh Mo₂C-A. The Mo/C of carbide phases (determined by XPS: degree of carburization) could have resulted in such performance differences between the two carbide catalysts. It is well known that the precious-metal-like character (*e.g.*, high hydrogenation activity) of Mo₂C catalysts increases with more complete carburization [16,26,31].

Despite the significant structural changes described earlier, the negative impact of hydrothermal aging on acetic acid conversion was minor. In fact, in the case of Mo₂C-B, the conversion at 250 °C actually doubled from 26 to 50% (Table 3). The intrinsic activity of Mo₂C-B degraded by 20%, but given that the BET surface area of Mo₂C-B increased upon aging, the net effect was that the rate per unit mass increased. For Ru/C the degradation in performance with aging seems to be mainly due to the loss in metallic surface area (*i.e.*, 50% decrease in dispersion + leaching), which attenuated the impact of the increased intrinsic rate.

Since the main objective of this reactor study was to determine if Mo carbides are catalytically active in the presence of liquid water and whether this activity are affected by hydrothermal aging, our discussion here is mainly focused on comparing the acetic acid conversion activity among different catalyst samples. We could, nonetheless, observe that ethanol was the major liquid product and that ethanol yield decreased with conversion and temperature. Consistent with the literature data [27,29], the formation of ethyl acetate (the product of an esterification reaction between ethanol and acetic acid) was low over Ru/C. In contrast, the formation of ethyl acetate was substantial over Mo₂C-B and did not change when conversion increased from 26 to 50%. The reason for this uniquely high selectivity to ethyl acetate over Mo₂C-B is not clear at this time, but could be explained in part by the surface bifunctionality of this catalyst (*i.e.*, the fact that MoC_x and MoO_x are both present). Indeed, it has been recently shown that combining Ru and acidic supports can significantly influence the carboxylic acid conversion chemistry [32], and metal oxide species created on carbide surfaces can act as acidic sites [33–37].

A large fraction of the acetic acid feed was apparently converted to gas products and CH₄ was qualitatively observed as a major product especially at high conversion (quantification was precluded by the instrumental limitations described in the Experimental section). High CH₄ formation over Ru/C catalysts at similar temperatures is well known and indicates C-C bond hydrogenolysis [28–30]. The aged Ru/C produced little liquid-phase product, suggesting the sensitivity of these acetic acid

conversion reactions to Ru particle size. To better assess the potential of Mo carbides in hydroprocessing bio-oils, the catalysts will need to be compared with Ru/C in converting more complex feedstock such as multi-compound models or real bio-oils. In addition, more complete product identification and quantification is necessary.

Table 3. Catalyst performance in aqueous-phase hydroprocessing of acetic acid; catalyst loading: 0.25 g, reaction mixture: 25 g of 10% (w/w) solution of acetic acid in water, reaction pressure: 2000 psig, stirring speed: 1000 rpm, reaction duration: 4 h.

Catalyst	Reaction temperature/°C	Acetic acid conversion/%	Selectivity to ethanol/%	Selectivity to ethyl acetate/%	Average rate of acetic acid conversion (areal) ^a / $\mu\text{mol m}^{-2}$
Mo ₂ C-A fresh	200	37	NM ^b	NM ^b	0.12
Mo ₂ C-A fresh	250	44	NM ^b	NM ^b	0.14
Mo ₂ C-A aged	250	40	NM ^b	NM ^b	0.07
Mo ₂ C-B fresh	250	26	70	12	0.50
Mo ₂ C-B aged	250	50	18	14	0.39
Ru/C fresh	200	61	28	4	0.39
Ru/C fresh	250	77	10	2	0.49
Ru/C aged	250	68	1	0	1.58

^a Rates normalized to BET surface area for Mo₂C and to metallic surface area estimated from TEM-measured particle size for Ru/C (for the aged Ru/C, *ca.* 55% loss of Ru due to leaching was taken into account based on XPS data shown in Table S2); ^b Not measured due to catalyst dissolution during the storage period between reactor evaluation and catalyst filtration.

3. Experimental Section

3.1. Catalysts

A standard temperature-programmed carburization method [18,37] was applied for the synthesis of Mo carbides. Ammonium heptamolybdate (Alfa Aesar, Heysham, UK) and a MoO₃ synthesized via a block copolymer templating method were used as precursors (the respective carburization products being denoted as Mo₂C-A and Mo₂C-B), while 15% CH₄/H₂ was used as the carburizing gas. After the synthesis (temperature ramping rate: 1 °C/min, final temperature: 700 °C, soak time: 1 h), the samples were passivated at room temperature in a 0.3% O₂/He flow. The block copolymer templating procedure used to prepare the MoO₃ precursor was adapted from a synthesis reported by Stucky and co-workers [38]. Briefly, 1 g of structure-directing copolymer Pluronic[®] P-123 (Aldrich, Steinheim, Germany) was dissolved in 10 g of anhydrous ethanol (99.5%, Acros Organics, Geel, Belgium). 0.01 moles of anhydrous MoCl₅ (99.6%, Alfa Aesar, Ward Hill, MA, USA) were then added to the resulting solution while the latter was vigorously stirred. The resulting mixture was subsequently allowed to age in a Petri dish at 60 °C for 15 days. Finally, the solids produced were calcined under static air at 300 °C for 2 h. 5 wt.% Ru/C (Alfa Aesar, Heysham, UK) was purchased and used as received for comparison purposes.

3.2. Hydrothermal Aging

Mo₂C and Ru/C samples were hydrothermally aged in a mechanically stirred 300 mL alloy C-276 batch reactor (Parr Instrument Co.). 2 g of sample was combined with 100 g of distilled water in the reactor. The air in the head space, as well as that dissolved in the water feed, was removed by evacuation and purging with N₂. The reactor was then filled with 95 psi of N₂ and heated to 250 °C under constant stirring at 1200 rpm. The final total pressure was approximately 690 psi at the aging temperature of 250 °C. After aging for 48 h, the solids were filtered and dried in air first at room temperature, then at 110 °C overnight.

3.3. Characterization

X-ray diffraction patterns were recorded on a powder X-ray diffractometer (X'Pert PRO, PANalytical, Almelo, The Netherlands) operated at 45 kV and 40 mA using CuK α radiation ($K_{\alpha} = 0.154178$ nm). The crystallite sizes (D_c) were estimated from the Scherrer equation using commercial software (HighScore Plus). The full width at half maximum (FWHM) and position of the peaks were calculated by profile fitting. Before the fitting, background and $K_{\alpha 2}$ of XRD peaks were removed and the peak broadening effect was adjusted using LaB6 as a standard sample. FWHM values of (101) and (110) planes and a shape factor of 0.94 were used.

Microscopic imaging of Mo samples was performed using a Hitachi HF3300 high-resolution transmission-scanning transmission electron microscope (TEM/STEM), which was operated at 300 kV. This instrument was also equipped with a secondary electron detector (SE) and a Bruker X-Flash silicon drift detector (SDD) for energy dispersive spectrometry (EDS). A Hitachi S-4800 Field Emission-Scanning Electron Microscope (FE-SEM) was used to collect micrographs of the Mo₂C samples at grain level. The internal powder microstructure was visualized using a Hitachi NB-5000 FIB-SEM (Focused Ion Beam-Scanning Electron Microscope). A high-milling-rate Ga ion beam was used to cut microscopic samples out of the powder grain revealing the interior porosity. Prior to milling, the region was locally coated with tungsten in order to protect the sample from the milling process. For the Ru/C catalyst, a JEOL 2200FS-AC Aberration-corrected STEM/TEM was used to measure the distribution of Ru particle sizes (more than 100 particles analyzed) before and after the hydrothermal aging. The calculated average particle sizes were then used to estimate Ru dispersion using a simple formula, dispersion = $0.9/D_p$ (D_p in nm) [39].

The specific surface area and porosity of catalyst samples were determined by measuring N₂ adsorption isotherms using an automatic volumetric adsorption apparatus (Quantachrome, Autosorb-1-C). Average particle sizes of Mo₂C catalysts were estimated from the equation $D_p = f/(\rho S_g)$ [39], where f is a shape factor and ρ is the density of Mo₂C (9.098 g/cc). A shape factor of 6 was applied assuming spherical or cubic Mo₂C particles [18].

Pulsed CO chemisorption was performed in a tubular fixed bed reactor (AMI-200, Altamira Instruments, Inc.) to measure the amount of irreversibly chemisorbed CO on Mo₂C. Before the measurements, passivated carbide samples were reduced in a flow of H₂ at 500 °C for 1 h, then cooled down to the chemisorption temperature (room temperature) in flowing Ar. A stoichiometry of Mo:CO

= 1:1 (*i.e.*, 1 molecule of CO per active site) was used to estimate the total number of active sites [18,40,41].

X-ray photoelectron spectroscopy was performed using a Thermo Scientific K-Alpha XPS instrument. The K-Alpha uses Al-K α x-rays focused to a spot 400 microns in diameter. Emitted photoelectrons were energy analyzed using a 180° double focusing hemispherical analyzer with a 128-channel detector. Survey data were collected at a pass energy of 200 eV and an energy resolution of 1 eV/step, while core level data were collected at 50 eV pass energy and 0.1 eV/step energy resolution. Sample charging was eliminated by using the K-Alpha's dual-beam charge compensation source, which uses both low energy Ar-ion and low energy electrons. An Ar-ion gun (operated at 2 kv) was used for *in-situ* cleaning of the sample surface. Data were collected and analyzed using the Avantage data system (v.4.61, Thermo Fisher Scientific, Waltham, MA, USA).

Thermogravimetric analysis (TGA) was carried out with a TA Instruments Q5000. The temperature was increased from room temperature to 800 °C at 10 °C/min in air (25 mL/min).

3.4. Reactor Evaluation

Catalyst performance was evaluated in a mechanically stirred 50 mL stainless-steel batch reactor. The catalyst (0.25 g) was reduced *in situ* at 250 °C under 50 psi of flowing H₂ for 2 h. After allowing the system to cool to room temperature, a vacuum was drawn on the reactor and 25 g of a 10% (*w/w*) solution of acetic acid in water was pulled into the reactor vessel. After purging with argon, the system was pressurized with H₂ to 1000 psig and heated to the reaction temperature while stirring the reaction mixture at 1000 rpm. Upon reaching the reaction temperature, which typically took ~15 min, the pressure was adjusted to 2000 psig and kept at this value throughout the experiment in order to replenish any hydrogen consumed by the reaction. After 4 h at the reaction temperature, the hydrogen line feeding the reactor was closed and the system was cooled to 35 °C prior to taking a gas sample for analysis. The system was then opened and its solid and liquid contents were collected. Only qualitative information could be obtained from gas analysis due to the fact that hydrogen (which was present in overwhelming excess) swamped the detector and precluded the quantification of gaseous products. The solids and liquids recovered were separated via gravimetric filtration prior to mixing a 1 g aliquot of the recovered liquid with 0.2 g of 2-butanol, which served as the internal standard. 0.2 μ L of the resulting solution were then analyzed on an Agilent 7890 GC equipped with a multimode inlet, a DB-Wax column (30 m \times 530 μ m \times 0.5 μ m) and a FID detector. Both the inlet and the FID were kept at a constant temperature of 240 °C, while the oven housing the column was programmed with a temperature ramp (10 °C/min) from 35 to 240 °C followed by an isotherm at the latter temperature lasting 9.5 min. The column was operated with a constant flow of 26 mL/min. Quantitative data were acquired using a 3-point calibration curve created using standards of ethanol and ethyl acetate. The linear calibration curve for each individual compound had an R^2 value of ≥ 0.99 . Acetic acid was quantified using CE (capillary electrophoresis, HP 1600).

4. Conclusions

We studied the structure of molybdenum carbides subjected to hot aqueous environments and their catalytic performance in aqueous-phase hydroprocessing of acetic acid. The results suggest that Mo

carbides have potential to be developed as hydrothermally stable catalysts, especially suitable for the low-temperature hydroprocessing of bio-oils, which is generally carried out using Ru/C-type catalysts. Key findings of the present study were:

- Bulk structures of Mo₂C were maintained after 48 h aging at 250 °C in liquid water;
- Carbide surfaces underwent significant structural changes during hydrothermal aging, particularly oxidation of carbidic Mo sites to oxidic sites, transformation of non-carbidic carbon species deposited during the carbide synthesis, and increased surface roughness;
- The removal of pore-blocking non-carbidic carbon and increased surface roughness during aging led to increased BET surface area;
- The extent of the structural changes observed during aging was sensitive to the initial carbide structure and was less severe under actual hydroprocessing conditions;
- Mo carbides showed excellent performance in the aqueous-phase hydroprocessing of acetic acid showing an intrinsic conversion activity comparable to that of Ru/C;
- The intrinsic activity of Mo carbides was shown to be sensitive to the carbide structure;
- Further investigation of carbide structures and performance in complex model or real bio-oil feedstock is needed to design robust, active, and inexpensive Mo carbide catalysts for bio-oil hydroprocessing.

Acknowledgments

This research was financially supported by the U.S. Department of Energy Bioenergy Technologies Office, the Laboratory Directed Research and Development Program of the Oak Ridge National Laboratory, and the University of Kentucky (Office of the Vice President for Research). A portion of this research was conducted at ORNL's Center for Nanophase Materials Sciences, which is a DOE Office of Science User Facility. The authors thank D. C. Elliott and T. R Hart at the Pacific Northwest National Laboratory for the useful discussion on the aqueous-phase aging and bio-oil evaluation approaches used in this study. Kevin Perrin, Jaime Shoup and Tonya Morgan at the University of Kentucky are thanked for their technical assistance.

Author Contributions

J.-S.C., V.S., E.S.-J. and M.C. conceived the research program and designed the experiments; V.S., E.S.-J., and J.-S.C. performed the catalyst synthesis and characterization; E.S.-J., S.A.L., and J.-S.C. carried out the reactor study of the catalysts including aging, acetic acid hydroprocessing and product analysis; M.J.L. and K.L.M. performed the microscopy; HMM performed the XPS; All contributed to the writing of the paper.

Conflicts of Interest

The authors declare no conflict of interest.

References

1. Czernik, S.; Bridgwater, A.V. Overview of applications of biomass fast pyrolysis oil. *Energy Fuels* **2004**, *18*, 590–598.
2. Connatser, R.M.; Lewis, S.A.L., Sr.; Keiser, J.R.; Choi, J.-S. Measuring bio-oil upgrade intermediates and corrosive species with polarity-matched analytical approaches. *Biomass Bioenergy* **2014**, *70*, 557–563.
3. Bartholomew, C.H.; Farrauto, R.J. *Fundamentals of Industrial Catalytic Processes*, 2nd ed.; John Wiley and Sons, Inc.: Hoboken, NJ, USA, 2006.
4. Bridgwater, A.V. Catalysis in thermal biomass conversion. *Appl. Catal. A* **1994**, *116*, 5–47.
5. Bridgwater, A.V. Production of high grade fuels and chemicals from catalytic pyrolysis of biomass. *Catal. Today* **1996**, *29*, 285–295.
6. Elliott, D.C. Historical developments in hydroprocessing bio-oils. *Energy Fuels* **2007**, *21*, 1792–1815.
7. Elliott, D.C.; Sealock, L.J., Jr.; Baker, E.G. Chemical processing in high-pressure aqueous environments. 2. Development of catalysts for gasification. *Ind. Eng. Chem. Res.* **1993**, *32*, 1542–1548.
8. Baker, E.G.; Elliott, D.C. Catalytic upgrading of biomass pyrolysis oils. In *Research in Thermochemical Biomass Conversion*; Bridgwater, A.V., Kuester, J.L., Eds.; Elsevier Science Publishers Ltd.: Barking, UK, 1988; pp. 883–895.
9. Zacher, A.H.; Olarte, M.V.; Santosa, D.M.; Elliott, D.C.; Jones, S.B. A review and perspective of recent bio-oil hydrotreating research. *Green Chem.* **2014**, *16*, 491–515.
10. Elliott, D.C.; Wang, H.; French, R.; Deutch, S.; Iisa, K. Hydrocarbon liquid production from biomass via hot-vapor-filtered fast pyrolysis and catalytic hydroprocessing of the bio-oil. *Energy Fuels* **2014**, *28*, 5909–5917.
11. Elliott, D.C.; Hart, T.R. Catalytic hydroprocessing of chemical models for bio-oil. *Energy Fuels* **2009**, *23*, 631–637.
12. Sinfelt, J.H.; Yates, D.J.C. Effect of carbiding on hydrogenolysis activity of molybdenum. *Nature Phys. Sci.* **1971**, *229*, 27–28.
13. Levy, R.B.; Boudart, M. Platinum-like behavior of tungsten carbide in surface catalysis. *Science* **1973**, *181*, 547–549.
14. Oyama, S.T. Preparation and catalytic properties of transition metal carbides and nitrides. *Catal. Today* **1992**, *15*, 179–200.
15. Lee, J.S.; Locatelli, S.; Oyama, S.T.; Boudart, M. Molybdenum carbide catalysts. 3. Turnover rates for the hydrogenolysis of n-butane. *J. Catal.* **1990**, *125*, 157–170.
16. Choi, J.-S.; Bugli, G.; Djéga-Mariadassou, G. Influence of the degree of carburization on the density of sites and hydrogenating activity of molybdenum carbides. *J. Catal.* **2000**, *193*, 238–247.
17. Volpe, L.; Boudart, M. Compounds of molybdenum and tungsten with high specific surface area. II. Carbides. *J. Solid State Chem.* **1985**, *59*, 348–356.
18. Lee, J.S.; Oyama, S.T.; Boudart, M. Molybdenum carbide catalysts. 1. Synthesis of unsupported powders. *J. Catal.* **1987**, *106*, 125–133.

19. Zhang, W.; Zhang, Y.; Zhao, L.; Wei, W. Catalytic activities of NiMo carbide supported on SiO₂ for the hydrodeoxygenation of ethyl benzoate, acetone, and acetaldehyde. *Energy Fuels* **2010**, *24*, 2052–2059.
20. Jongerijs, A.L.; Gosselink, R.W.; Dijkstra, J.; Bitter, J.H.; Bruijninx, P.C.A.; Weckhuysen, B.M. Carbon nanofiber supported transition-metal carbide catalysts for the hydrodeoxygenation of guaiacol. *ChemCatChem* **2013**, *5*, 2964–2972.
21. Yu, W.; Saliccioli, M.; Xiong, K.; Barteau, M.A.; Vlachos, D.G.; Chen, J.G. Theoretical and experimental studies of C–C versus C–O bond scission of ethylene glycol reaction pathways via metal-modified molybdenum carbides. *ACS Catal.* **2014**, *4*, 1409–1418.
22. Xiong, K.; Lee, W.-S.; Bhan, A.; Chen, J.G. Molybdenum carbide as a highly selective deoxygenation catalyst for converting furfural to 2-methylfuran. *ChemSusChem* **2014**, *7*, 2146–2151.
23. Rerez-Romo, P.; Potvin, C.; Manoli, J.-M.; Chehimi, M.M.; Djéga-Mariadassou, G. Phosphorus-doped molybdenum oxynitrides and oxygen-modified molybdenum carbides: synthesis, characterization, and determination of turnover rates for propene hydrogenation. *J. Catal.* **2002**, *208*, 187–196.
24. Ravenelle, R.M.; Copeland, J.R.; Kim, W.-G.; Crittenden, J.C.; Sievers, C. Structural changes of γ -Al₂O₃-supported catalysts in hot liquid water. *ACS Catal.* **2011**, *1*, 552–561.
25. Wu, W.; Wu, Z.; Liang, C.; Ying, P.; Feng, Z.; Li, C. An IR study on the surface passivation of Mo₂C/Al₂O₃ catalyst with O₂, H₂O and CO₂. *Phys. Chem. Chem. Phys.* **2004**, *6*, 5603–5608.
26. Choi, J.-S.; Krafft, J.-M.; Krzton, A.; Djéga-Mariadassou, G. Study of residual oxygen species over molybdenum carbide prepared during in situ DRIFTS experiments. *Catal. Lett.* **2002**, *81*, 175–180.
27. Ravenelle, R.M.; Copeland, J.R.; van Pelt, A.H.; Crittenden, J.C.; Sievers, C. Stability of Pt/ γ -Al₂O₃ catalysts in model biomass solutions. *Top. Catal.* **2012**, *55*, 162–174.
28. Elliott, D.C.; Hart, T.R.; Neuenschwander, G.G. Chemical processing in high-pressure aqueous environments. 8. Improved catalysts for hydrothermal gasification. *Ind. Eng. Chem. Res.* **2006**, *45*, 3376–3781.
29. Olcay, H.; Xu, L.; Xu, Y.; Huber, G.W. Aqueous-phase hydrogenation of acetic acid over transition metal catalysts. *ChemCatChem* **2010**, *2*, 1420–1424.
30. Wan, H.; Chaudhari, R.V.; Subramaniam, B. Aqueous phase hydrogenation of acetic acid and its promotional effect on *p*-cresol hydrodeoxygenation. *Energy Fuels* **2013**, *27*, 487–493.
31. Lee, J.S.; Yeom, M.H.; Park, K.Y.; Nam, I.-S.; Chung, J.S.; Kim, Y.G.; Moon, S.H. Preparation and benzene hydrogenation activity of supported molybdenum carbide catalysts. *J. Catal.* **1991**, *128*, 126–136.
32. Chen, L.; Zhu, Y.; Zheng, H.; Zhang, C.; Zhang, B.; Li, Y. Aqueous-phase hydrodeoxygenation of carboxylic acids to alcohols or alkanes over supported Ru catalysts. *J. Mol. Catal. A* **2011**, *351*, 217–227.
33. Pham-Huu, C.; Ledoux, M.J.; Guille, J. Reactions of 2- and 3-methylpentane, methylcyclopentane, cyclopentane, and cyclohexane on activated Mo₂C. *J. Catal.* **1993**, *143*, 249–261.
34. Blekkan, E.A.; Pham-Huu, C.; Ledoux, M.J.; Guille, J. Isomerization of *n*-heptane on an oxygen-modified molybdenum carbide catalyst. *Ind. Eng. Chem. Res.* **1994**, *33*, 1657–1664.

35. Ledoux, M.J.; del Gallo, P.; Pham-Huu, C.; York, A.P.E. Molybdenum oxycarbide isomerization catalysts for cleaner fuel production. *Catal. Today* **1996**, *27*, 145–150.
36. Iglesia, E.; Ribeiro, F.H.; Boudart, M.; Baumgartner, J.E. Synthesis, characterization, and catalytic properties of clean and oxygen-modified tungsten carbides. *Catal. Today* **1992**, *15*, 307–337.
37. Ribeiro, F.H.; Betta, R.A.D.; Guskey, G.J.; Boudart, M. Preparation and surface composition of tungsten carbide powders with high specific surface area. *Chem. Mater.* **1991**, *3*, 805–812.
38. Yang, P.; Zhao, D.; Margolese, D.I.; Chmelka, B.F.; Stucky, G.D. Block copolymer templating syntheses of mesoporous metal oxides with large ordering lengths and semicrystalline framework. *Chem. Mater.* **1999**, *11*, 2813–2826.
39. Boudart, M.; Djéga-Mariadassou, G. *Kinetics of Heterogeneous Catalytic Reactions*; Princeton University Press: Princeton, NJ, USA, 1984; pp. 25–26.
40. Ramanathan, S.; Oyama, S.T. New catalysts for hydroprocessing: transition metal carbides and nitrides. *J. Phys. Chem.* **1995**, *99*, 16365–16372.
41. St. Clair, T.P.; Dhandapani, B.; Oyama, S.T. Cumene hydrogenation turnover rates on Mo₂C: CO and O₂ as probes of the active site. *Catal. Lett.* **1999**, *58*, 169–171.

© 2015 by U.S. Government; licensee MDPI, Basel, Switzerland. This article is an open access article distributed under the terms and conditions of the Creative Commons Attribution license (<http://creativecommons.org/licenses/by/4.0/>).